AD

Technical Report ARAEW-TR-04012

Characterization of Niobium, Tantalum and Chromium Sputtered Coatings on Steel Using Eddy Currents

Chris Mulligan, Changqing Lee, Yaron Danon

SEPTEMBER 2004

ARMAMENT RESEARCH, DEVELOPMENT AND ENGINEERING CENTER
Armaments Engineering & Technology Center
Weapon Systems & Technology

Approved for public release; distribution is unlimited.

The views, opinions, and/or findings contained in this report are those of the author(s) and should not be construed as an official Department of the Army position, policy, or decision, unless so designated by other documentation.

The citation in this report of the names of commercial firms or commercially available products or services does not constitute official endorsement by or approval of the U.S. Government.

Destroy this report when no longer needed by any method that will prevent disclosure of its contents or reconstruction of the document. Do not return to the originator.

REPORT DOCUMENTATION PAGE

Form Approved
OMB No. 0704-0188

1. REPORT DATE *(DD-MM-YYYY)*	2. REPORT TYPE	3. DATES COVERED *(From - To)*
Sept 2004	FINAL	

4. TITLE AND SUBTITLE
Characterization of Niobium, Tantalum and Chromium Sputtered Coatings on Steel Using Eddy Currents

5a. CONTRACT NUMBER

5b. GRANT NUMBER

5c. PROGRAM ELEMENT NUMBER

6. AUTHOR(S)
Chris Mulligan, Changqing Lee*, Yaron Danon*

5d. PROJECT NUMBER

5e. TASK NUMBER

5f. WORK UNIT NUMBER

7. PERFORMING ORGANIZATION NAME(S) AND ADDRESS(ES)
U.S. Army ARDEC
Benet Laboratories, RDAR-WSB
Watervliet, NY 12189-4000

8. PERFORMING ORGANIZATION REPORT NUMBER
ARAEW-TR-04012

9. SPONSORING/MONITORING AGENCY NAME(S) AND ADDRESS(ES)
U.S. Army ARDEC
Benet Laboratories, RDAR-WSB
Watervliet, NY 12189-4000

10. SPONSOR/MONITOR'S ACRONYM(S)

11. SPONSORING/MONITORING AGENCY REPORT NUMBER

12. DISTRIBUTION AVAILABILITY STATEMENT
Approved for public release; distribution is unlimited.

13. SUPPLEMENTARY NOTES
Department of Mechanical, Aerospace and Nuclear Engineering, Rensselaer Polytechnic Institute, Troy, NY 12180

14. ABSTRACT
A method that uses induced eddy current for characterization of niobium, tantalum and chromium sputtered coating on steel is presented in this paper. The objective of this work is to find the correlation between the sputtering conditions and resistivity of coatings and to develop a system for fast inspection of coatings as a coating quality control tool during production as well as in the field for determining coating degradation levels. A two-probe differential system having higher sensitivity and less noise than a one-probe system with 2D scanning ability was developed. A computer program that controls an XY table and performs fast data acquisition was written. Resistivity maps of the niobium, tantalum and chromium coated samples were constructed and are shown in the paper.

15. SUBJECT TERMS
Eddy currents; Sputtered coatings; Resistivity of coatings; Sputtering conditions

16. SECURITY CLASSIFICATION OF:			17. LIMITATION OF ABSTRACT	18. NUMBER OF PAGES	19a. NAME OF RESPONSIBLE PERSON
a. REPORT	b. ABSTRACT	c. THIS PAGE	U	15	Chris Mulligan
U/U	U	U			19b. TELEPONE NUMBER (*Include area code*) 518-266-5415

INSTRUCTIONS FOR COMPLETING SF 298

1. REPORT DATE. Full publication date, including day, month, if available. Must cite at lest the year and be Year 2000 compliant, e.g., 30-06-1998; xx-08-1998; xx-xx-1998.

2. REPORT TYPE. State the type of report, such as final, technical, interim, memorandum, master's thesis, progress, quarterly, research, special, group study, etc.

3. DATES COVERED. Indicate the time during which the work was performed and the report was written, e.g., Jun 1997 - Jun 1998; 1-10 Jun 1996; May - Nov 1998; Nov 1998.

4. TITLE. Enter title and subtitle with volume number and part number, if applicable. On classified documents, enter the title classification in parentheses.

5a. CONTRACT NUMBER. Enter all contract numbers as they appear in the report, e.g. F33615-86-C-5169.

5b. GRANT NUMBER. Enter all grant numbers as they appear in the report, e.g. 1F665702D1257.

5c. PROGRAM ELEMENT NUMBER. Enter all program element numbers as they appear in the report, e.g. AFOSR-82-1234.

5d. PROJECT NUMBER. Enter al project numbers as they appear in the report, e.g. 1F665702D1257; ILIR.

5e. TASK NUMBER. Enter all task numbers as they appear in the report, e.g. 05; RF0330201; T4112.

5f. WORK UNIT NUMBER. Enter all work unit numbers as they appear in the report, e.g. 001; AFAPL30480105.

6. AUTHOR(S). Enter name(s) of person(s) responsible for writing the report, performing the research, or credited with the content of the report. The form of entry is the last name, first name, middle initial, and additional qualifiers separated by commas, e.g. Smith, Richard, Jr.

7. PERFORMING ORGANIZATION NAME(S) AND ADDRESS(ES). Self-explanatory.

8. PERFORMING ORGANIZATION REPORT NUMBER. Enter all unique alphanumeric report numbers assigned by the performing organization, e.g. BRL-1234; AFWL-TR-85-4017-Vol-21-PT-2.

9. SPONSORING/MONITORS AGENCY NAME(S) AND ADDRESS(ES). Enter the name and address of the organization(s) financially responsible for and monitoring the work.

10. SPONSOR/MONITOR'S ACRONYM(S). Enter, if available, e.g. BRL, ARDEC, NADC.

11. SPONSOR/MONITOR'S REPORT NUMBER(S). Enter report number as assigned by the sponsoring/ monitoring agency, if available, e.g. BRL-TR-829; -215.

12. DISTRIBUTION/AVAILABILITY STATEMENT. Use agency-mandated availability statements to indicate the public availability or distribution limitations of the report. If additional limitations/restrictions or special markings are indicated, follow agency authorization procedures, e.g. RD/FRD, PROPIN, ITAR, etc. Include copyright information.

13. SUPPLEMENTARY NOTES. Enter information not included elsewhere such as: prepared in cooperation with; translation of; report supersedes; old edition number, etc.

14. ABSTRACT. A brief (approximately 200 words) factual summary of the most significant information.

15. SUBJECT TERMS. Key words or phrases identifying major concepts in the report.

16. SECURITY CLASSIFICATION. Enter security classification in accordance with security classification regulations, e.g. U, C, S, etc. If this form contains classified information, stamp classification level on the top and bottom of this page.

17. LIMITATION OF ABSTRACT. This block must be completed to assign a distribution limitation to the abstract. Enter UU (Unclassified Unlimited) or SAR (Same as Report). An entry in this block is necessary if the abstract is to be limited.

Characterization of Niobium, Tantalum and Chromium Sputtered Coatings on Steel Using Eddy Currents

Chris Mulligan[1], Changqing Lee*, and Yaron Danon*

[1] Benet Laboratories, US Army, AMSTA-AR-CCB-TB, Watervliet Arsenal, NY 12189

* Department of Mechanical, Aerospace and Nuclear Engineering, Rensselaer Polytechnic Institute, Troy, NY 12180

Abstract

A method that uses induced eddy current for characterization of niobium, tantalum and chromium sputtered coating on steel is presented in this paper. The objective of this work is to find the correlation between the sputtering conditions and resistivity of coatings and to develop a system for fast inspection of coatings as a coating quality control tool during production as well as in the field for determining coating degradation levels. A two-probe differential system having higher sensitivity and less noise than a one-probe system with 2D scanning ability was developed. A computer program that controls an XY table and performs fast data acquisition was written. Resistivity maps of the niobium, tantalum and chromium coated samples were constructed and are shown in the paper. For niobium coatings, the relationship between sputtering pressure and resistivity of coatings is examined, as well as the relationship between impurity level of process gas and resistivity of coatings. For tantalum coatings, the relationship between beta-Ta fraction and resistivity are analyzed. For chromium coatings, the relationship between micro-crack density and resistivity of coatings are analyzed. The topographic picture and destructive analysis of the samples show very good correlation with eddy currents measurements.

I. Introduction

The eddy current method can be applied to measure electrical resistivity and thickness of thin coatings on metallic material [1][2]. As a method for non-destructive inspection, eddy current techniques are also used for detection of corrosion in airplane structures and defects in metals [3]-[5]. Recently we also reported an application for coating surface inspection [6][7].

Currently, the demand to increase range, rate of fire, and muzzle velocity has resulted in increased wear and erosion problems in gun tubes. As a result there has been a drive to introduce improved coatings to mitigate these problems. In support of this research, use of nondestructive eddy current techniques to characterize the structure and properties of coatings will help to advance the development and maturation of the next generation of advanced coatings for gun tubes.

The eddy current method is based on the induction of magnetic fields in a sample. These magnetic fields created by a coil will induce currents in the metal, which can be detected by a probe above the metal surface [8]. In the work described here we use the same probe to induce the magnetic field and detect the eddy currents. The net effect of this process is to measure the change of the probe's impedance when it is coupled to the metallic surface under testing.

The eddy current technique has several advantages, it is a nondestructive and non-contact method, and as a result, no damage is done to the surface even when the scan is performed at very high speeds.

Thus, it does not rely on good contact with the surface like other resistivity measurement methods such as a four-point probe. The method can accurately determine the resistivity and in some configurations also measure the coating thickness. Another advantage is that the instrumentation required for these types of testing is relatively simple and thus reliable and inexpensive.

Resistivity measurement is of special interest due to its relationship with factors affecting coating properties. For instance, the resistivity of coatings is very sensitive to changes in density and morphology. In fact, porous zone 1 deposited coatings can have resistivities an order of magnitude or greater than the respective bulk values for a given material [9]. In addition, resistivity is sensitive to interstitial impurities such as H, O, C, and N.

Besides these relationships, in physical vapor deposited coatings, multiple phases of some materials may form with varying resistivities. This is the case for one of the primary materials under consideration for gun bore protection. The refractory metal tantalum can form two phases under physical vapor deposition**,** the alpha (α) phase, which is the stable bcc phase and beta (β), which is a metastable phase. In tantalum deposited on steel, the beta (β) phase tends to form at the substrate/coating interface where adhesion is critical. This is problematic in that the beta phase is very brittle and may result in premature coating failure under applied stresses. It has been reported [7][10] that beta tantalum has a resistivity an order of magnitude greater than alpha phase tantalum (~200 $\mu\Omega$-cm and ~20 $\mu\Omega$-cm respectively). Taking this into account, it is easily perceived that an instrument that can measure the resistivity of tantalum coatings would be the most practical characterization device. Electrical resistivity measurements have been very effective for research in process control in fabrication of micro-electronic circuits [12]. However, in this application, the coating is deposited onto a conductive substrate (gun steel as opposed to silicon); therefore, measuring resistivity through traditional four-point probe measurements is not possible.

The current practice to identify and quantify concentrations of beta tantalum is through X-Ray diffraction, by which direct information on the crystalline structure can be obtained [11] and/or destructive characterization. However, these methods are relatively slow, more costly, and much more difficult to execute than the method proposed by the authors, particularly outside of the lab environment.

II. THEORY

The theory of eddy current testing can be derived from Maxwell's equations. The analytical solution for an air coil positioned above a one-layer coated substrate as illustrated in Figure 1 was given by [13].

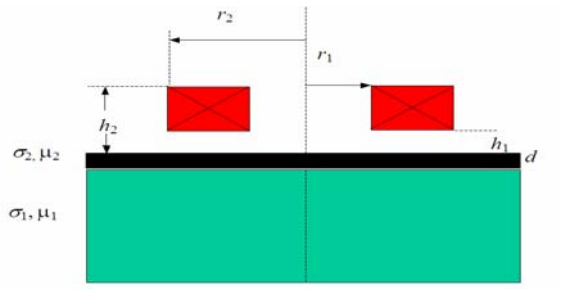

Figure 1 An air coil over one layer coating of thickness d

The coil inner radius is noted by r_1 and the outer radius is noted by r_2. The bottom and top distance of the coil edges from the coating are h_1 and h_2 respectively such that the coil length is given by $L = h_2 - h_1$. The number of turns of the coil is denoted by n. σ_1 and σ_2 are the conductivity of the coating and the substrate respectively. μ_1 and μ_2 are the permeability of coating and the substrate respectively. The thickness of the coatings is denoted by d.

The expression of the coil's impedance Z(ω) given by [13] is applicable for a single excitation frequency. A method that is better suited for fast sampling of the impedance is the pulsed eddy current. The pulsed eddy current technique, which uses a step function voltage to excite the probe, is a promising approach in the field of eddy current testing. The advantage of using a step function voltage is that it contains a continuum of frequencies; as a result, the electromagnetic response to several different frequencies can be measured with just a single pulse. Since the skin depth of penetration is dependent on the frequency of excitation, information from a range of depths can be obtained simultaneously. For example Tai et al. [2] showed that pulsed eddy current could be used to simultaneously determine the resistivity and thickness of coatings on non-magnetic substrates. However for the work presented here, we chose to simplify the procedure and measured the thickness of the tantalum coating with the magnetic induction method. Another advantage of applying pulsed eddy currents for the purpose of repetitive scanning is that the low duty cycle of the pulses puts less average power through the small probe coils, which allows to operate at high instantaneous current during the pulse itself. For the pulsed eddy current technique, the coil will be excited by a square pulse of duration t_p during which we apply constant voltage V_0 to the coil. This is illustrated in Figure 2.

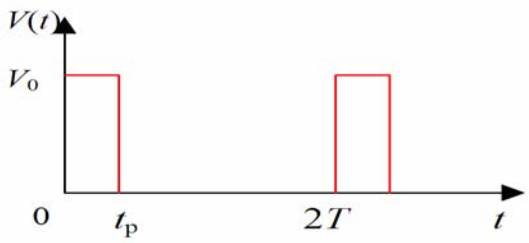

Figure 2 Square excitation pulse with width t_p, height V_0 repeating every 2T.

In order to apply the theory developed for the impedance calculations of a coil excited by a pulse, we can first apply Fourier transformation to obtain all of the components of the pulse. After that, we can get the response of the coil from all the components. These components are added and the response of a pulse is obtained. The detailed process is given as follows.

First, a Fourier transformation of the pulse (see Figure 2) is used.

$$V(t) = V_0\left[\frac{t_p}{2T} + \sum_{n=1}^{N}\left(a_n \cos(\omega_n t) + b_n \sin(\omega_n t)\right)\right] \quad (1)$$

Where the Fourier coefficients a_n and b_n are given by;

$$a_n = \frac{\sin(\omega_n t_p)}{n\pi} \quad (2)$$

$$b_n = \frac{1-\cos(\omega_n t_p)}{n\pi} \tag{3}$$

The angular frequency and frequency are given by $\omega_n = n\pi/T$ and $f_n = \omega_n/(2\pi)$ respectively. To calculate the voltage on the coil, consider the circuit in Figure 3. Applying the relation $I=V(t)/Z(\omega)$ and using Equation (1), the voltage that is read by the A/D board is given by,

$$V(t) = V_0 R_L \cdot \left[\frac{t_p}{2TR_T} + \sum_{n=1}^{N} \left(\frac{a_n \cos(\omega_n t - \theta(\omega_n)) + b_n \sin(\omega_n t - \theta(\omega_n))}{Mag(\omega_n)} \right) \right] \tag{4}$$

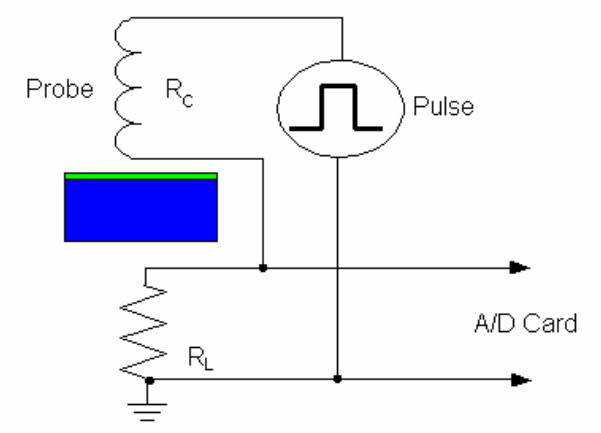

Figure 3. Experiment setup for a one-coil system shown above a one-layer coated sample

where $Z(\omega)$ is the impedance of the coil for each frequency, R_T is the total resistance in the circuit, including the load resistance R_L, the coil resistance R_C, and the output resistance of the pulse generator R_0. In this case the complex impedance of the coil and the real resistance of the other components were represented in polar coordinates with magnitude:

$$Mag(\omega_n) = \sqrt{\mathrm{Im}(Z(\omega_n))^2 + [\mathrm{Re}(Z(\omega_n)) + R_t]^2} \tag{5}$$

and phase,

$$\theta(\omega_n) = \tan^{-1}\left(\frac{\mathrm{Im}(Z(\omega_n))}{\mathrm{Re}(Z(\omega_n)) + R_t} \right) \tag{6}$$

To achieve high sensitivity, two measurements are done. One over the sample coatings is labeled S and another over the reference substrate is labeled R. The difference is given by

$$\Delta V(t) = V_S(t) - V_R(t) \tag{7}$$

The advantage of this method is that allows to differentiate a small signal $\Delta V(t)$ that is embedded in the large signal from the coil response $V_S(t)$.

III. Experiment Setup

A differential system with two coils was used and is shown in Figure 4. The differential system was driven by a Tabor-8024 waveform /function generator, and the signal is amplified by a wide band

differential amplifier that was designed by the authors for this purpose. The gain of the amplifier is changeable and a factor of 5 is applied in the experiment. The output of the amplifier was connected to a 14-bit A/D card (CompuScope 14100) from Gage Applied.

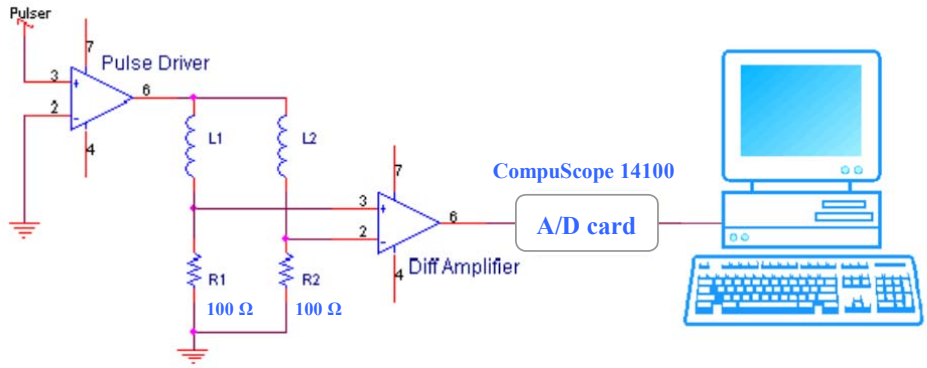

Figure 4 Experimental setup for the differential system included probe coils, pulse driver, differential amplifier and a computer DAQ

The pulse driver was designed to provide the system with constant voltage with a very low internal resistance, less than 1Ω.

In order to map the resistivity of a sample, an eddy current scanner was designed and constructed and is illustrated in Figure 5. One sample was positioned on a computer controlled XY table and another reference sample was used as illustrated in Figure 5. The two coils are stationary and the sample being scanned is moving under the scanning probe. This arrangement allows the system to scan the resistivity of the sample relative to the resistivity of the magnetic gun steel when it is used as the reference sample. In order to reduce inaccuracies from small differences between the two differential channels, a measurement of the system's response when the two probes are placed over stainless steel was done first. This measurement is treated as background and was subtracted from the signal obtained from each pulse. The typical height of the probe above the surface h_1=0.5mm.

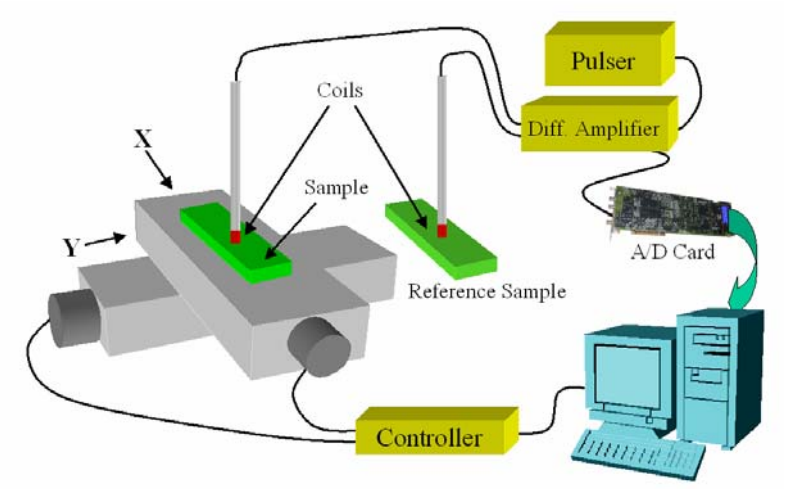

Figure 5. An illustration of the XY eddy current scanner. The scanner includes an XY positioning system and a differential probe system

Depositions of tantalum, niobium, and chromium were completed on 4340 steel substrates via magnetron sputtering and electroplating. The stainless steel deposition chamber consists of a plasma cleaning station and a 2 inch diameter standard water-cooled magnetron gun. Background pressures were measured via an Inficon residual gas analyzer.

Preparation of the substrates prior to installation into the system included polishing to 2 – 3 μinch RMS surface finish. Directly prior to magnetron sputtering of each tantalum and niobium coating, the substrates were plasma cleaned in-situ in Ar at a rate of ~170 Å/min for 30 minutes to ensure good bonding.

The parameters of each deposition are given in Table I. Niobium was used on several depositions in lieu of tantalum due to its close relationship with tantalum and the fact that it does not form the detrimental beta phase. This allows us to differentiate and test such parameters as sputtering pressure, contamination levels, etc. without worrying about the formation of beta phase, which is unpredictable in tantalum and can change with the aforementioned sputtering parameters.

Table I: Test samples and deposition parameters

Series	Material	Sample	Sputtering Pressure (mT)	Sputtering Gas	Impurity Levels (% Process Gas)*	Coating Thickness (μm)
Impurity	Nb	Nb-A1	10	Ar	10%	40.9
Level	Nb	Nb-A2	10	Ar	5%	16.4
Sputtering	Nb	Nb-1	10	Ar	1.5%	49.5
Pressure	Nb	Nb-2	30	Ar	1.5%	62.0
	Nb	Nb-3	40	Ar	1.5%	38.1
Aqueous	HC-Cr	Cr-1	Plated	--	--	43.2
HC-Cr	HC-Cr	Cr-2	Plated	--	--	71.1
	HC-Cr	Cr-3	Plated	--	--	88.9
	HC-Cr	Cr-4	Plated	--	--	137.2
Beta-Ta	Ta	Ta-1	30	Kr	1.5%	29.5
Fraction	Ta	Ta-2	10	Kr	1.5%	31.2

* As measured with an Inficon Residual Gas Analyzer.

To determine the sensitivity of resistivity measurement to coating density, niobium depositions were completed at different sputtering pressures. The effects of sputtering pressure on coating density are related to atomic shadowing and increased sputtered particle collisions in the gas phase and are relatively well understood [14][15]. Depositions at 10, 30, and 40 mT were completed. The current was held constant with each run, however there were some fluctuations in voltage and power and thus substrate temperature with increasing pressure. The temperature was monitored and based on the relatively small changes in homologous temperatures (T/T_m), it is reasonable to assume the temperature change does not play a substantial role in coating density.

To evaluate the sensitivity of eddy current resistivity measurement to impurity content, two

niobium depositions were completed at 10 mT Ar sputtering pressure with the introduction of a controlled leak through a bleed valve on the vacuum system. The partial pressure of the background gas in relation to the sputtering gas was monitored using an Inficon Residual Gas Analyzer (RGA). The first deposition was completed with a background gas partial pressure of 10% total (or 1.0 mT) and the second deposition was completed with a background gas partial pressure of 5% (or 0.5 mT). A background gas pressure of any higher value would lead to the risk of poisoning the target and would not be a realistic representation of the level of background impurities that may be present during an actual deposition.

To determine the relationship between resistivity and beta-Ta concentration, tantalum depositions were completed in a similar manner with the following exceptions. Krypton as opposed to Argon sputtering gas was used due to the increase in beta-Ta concentration experienced in this system while sputtering in Kr. The tantalum specimen dimension was increased to 4.0” in length due to the geometry of the beta-Ta that is formed. The beta-Ta (lighter phase) tends to form directly in the center of the specimen and there is a gradual transition to alpha-Ta (darker phase) away from the center as illustrated in Figure 6. This gives us a full range of beta-Ta concentrations to evaluate via eddy currents.

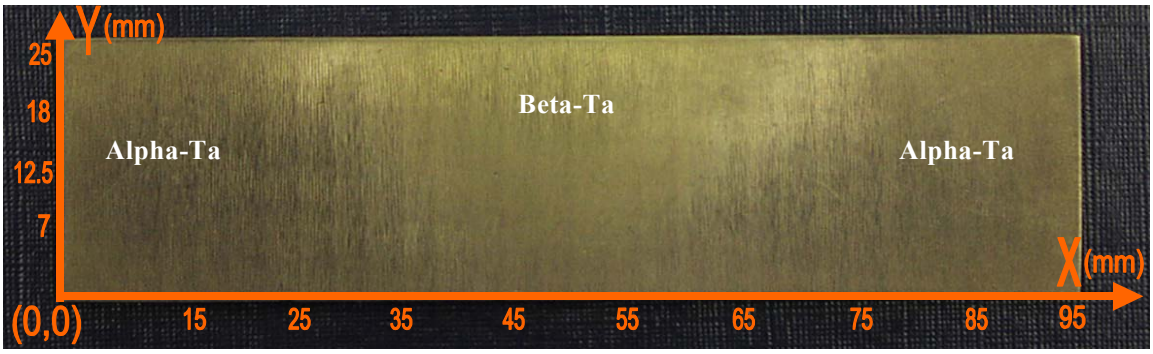

Figure 6. Surface image illustrating the distribution of alpha (darker phase) and beta (lighter phase) tantalum across the surface of the sample.

To determine the relationship between micro-crack density and resistivity in electroplated chromium coatings, four depositions were completed of varying thickness. The depositions were completed in a bath at 55C and a deposition rate of 12 – 15 μm/hr. The resultant coatings contain varying concentrations of micro-cracks which are related to the coating thickness.

IV. Results

For the niobium sample, an accurate thickness measurement was completed using a magnetic induction coating thickness gauge from DeFelsko. The measurement does not depend on the resistivity of the coating. The measurements were completed on a grid overlaid on the sample as shown in Figure 7. A total of 9 points were measured. The thickness at an arbitrary point is obtained by linear interpolation between measured points as shown in Figure 8. This method is sufficiently accurate when the changes in thickness are small and vary smoothly, which is typical for the samples analyzed in this work.

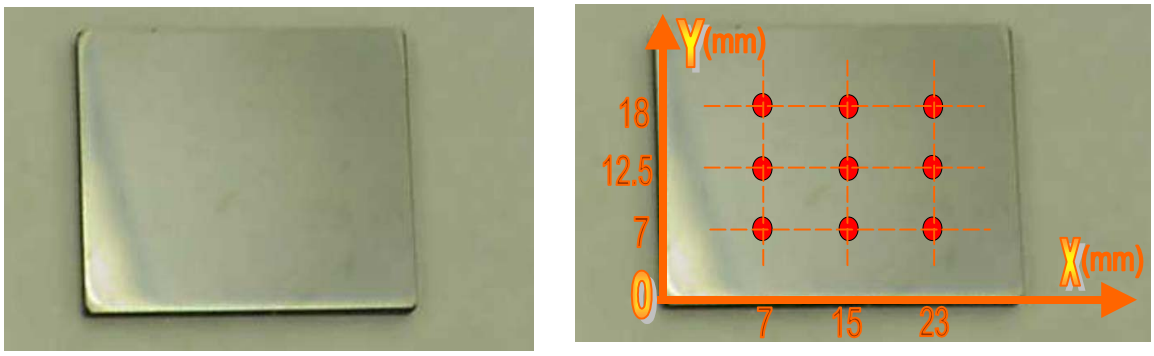

(a) (b)

Figure 7 (a) Typical planar niobium sample deposited via magnetron sputtering, (b) niobium sample with an imaginary grid showing thickness measurement points

Figure 8 illustrates the thickness map along the surface of the niobium coating that is generated from the linear interpolation of points measured via magnetic induction.

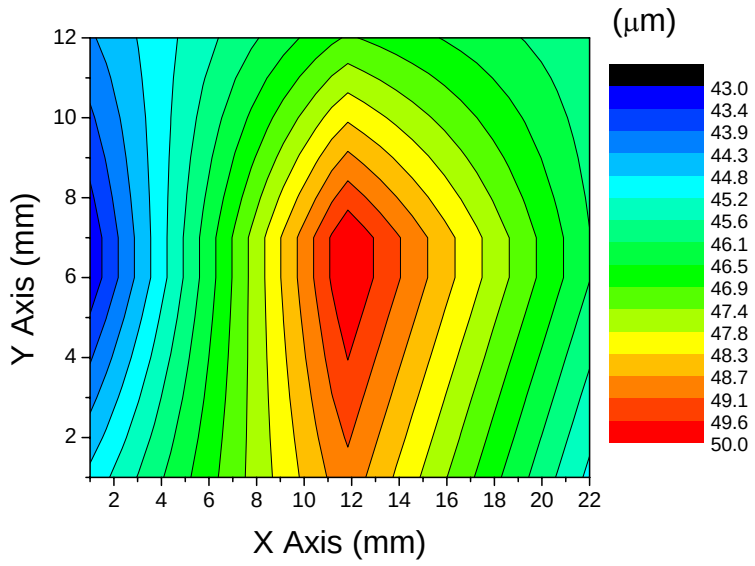

Figure 8 Thickness map for the niobium sample as measured via a magnetic induction thickness gauge (Sample Nb-1)

Figure 9 shows a resistivity map of a niobium sample that was obtained using our eddy current scanning system and was corrected for coating thickness nonuniformity.

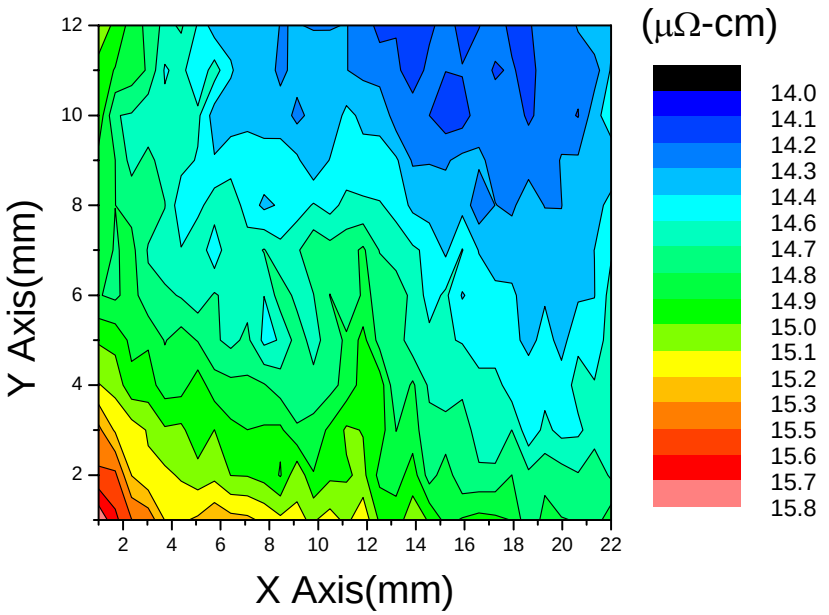

Figure 9 Resistivity map as measured via eddy current for the niobium sample (Nb-1). Measurement was corrected for changes in the coating thickness.

IV.1 The relationship between sputtering pressure and resistivity of coatings for niobium coatings

Three specimens (Nb-1, 2, and 3) were deposited to test the correlation of resistivity and coating density. For these three Niobium specimens, the thickness as measured by magnetic induction and the resistivity as measured by eddy current along the surface are relatively uniform. This was expected due to the fact that niobium does not form a secondary metastable phase.

Surface images and heightmaps were taken of each specimen prior to subjecting to eddy current measurement. Composite images were produced for clearer description. These are given in Figure 10 with the optical image on the left and the associated heightmap given on the right. The surface structures correlate well with the measured changes in resistivity. As illustrated, the change in surface structure is not as drastic as one increases pressure to 30 mT as opposed to 40 mT. Inset in the images are the relative rms surface roughnesses given in arbitrary units as measured by laser scanning confocal microscopy.

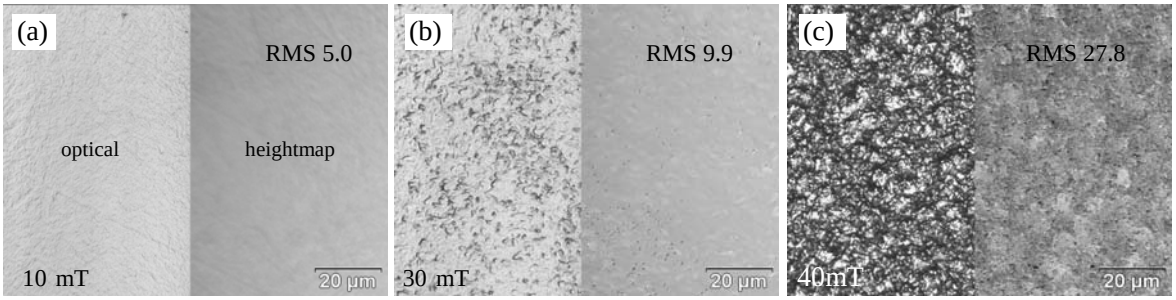

Figure 10. Composite images combining optical (left) and topographic heightmap (right) images as measured by laser scanning confocal microscopy. The sputtering pressure and surface finish are given for each image. Note the increase in surface roughness with increasing sputtering pressure (RMS surface finish given in a.u.).

Furthermore, metallographic characterization of the specimens was conducted to compare resistivity values to actual structural changes. Illustrated in Figure 11 is the plot of resistivity vs. sputtering pressure and superimposed are cross-sectional images taken from the niobium sputtered specimens following a 90 second etch in HF-H_2SO_4 etchant. The results are similar to that of the topographic analysis. The porosity noted at 40 mT is much more acute than that at 30 mT, which is in agreement with the resistivity measurements. The greater variation in the resistivity across the surface of the sample sputtered at 40 mT is not believed to be representative of fluctuations in the measurement system but rather actual fluctuations in the resistivity of the coating. At 40 mT the atomic shadowing effects are exacerbated and since a 2 inch diameter magnetron gun was used, the coating exhibits highest resistivity at the center point and lower resistivity at the edges as the oblique flux component plays more of a role in the shadowing effect.

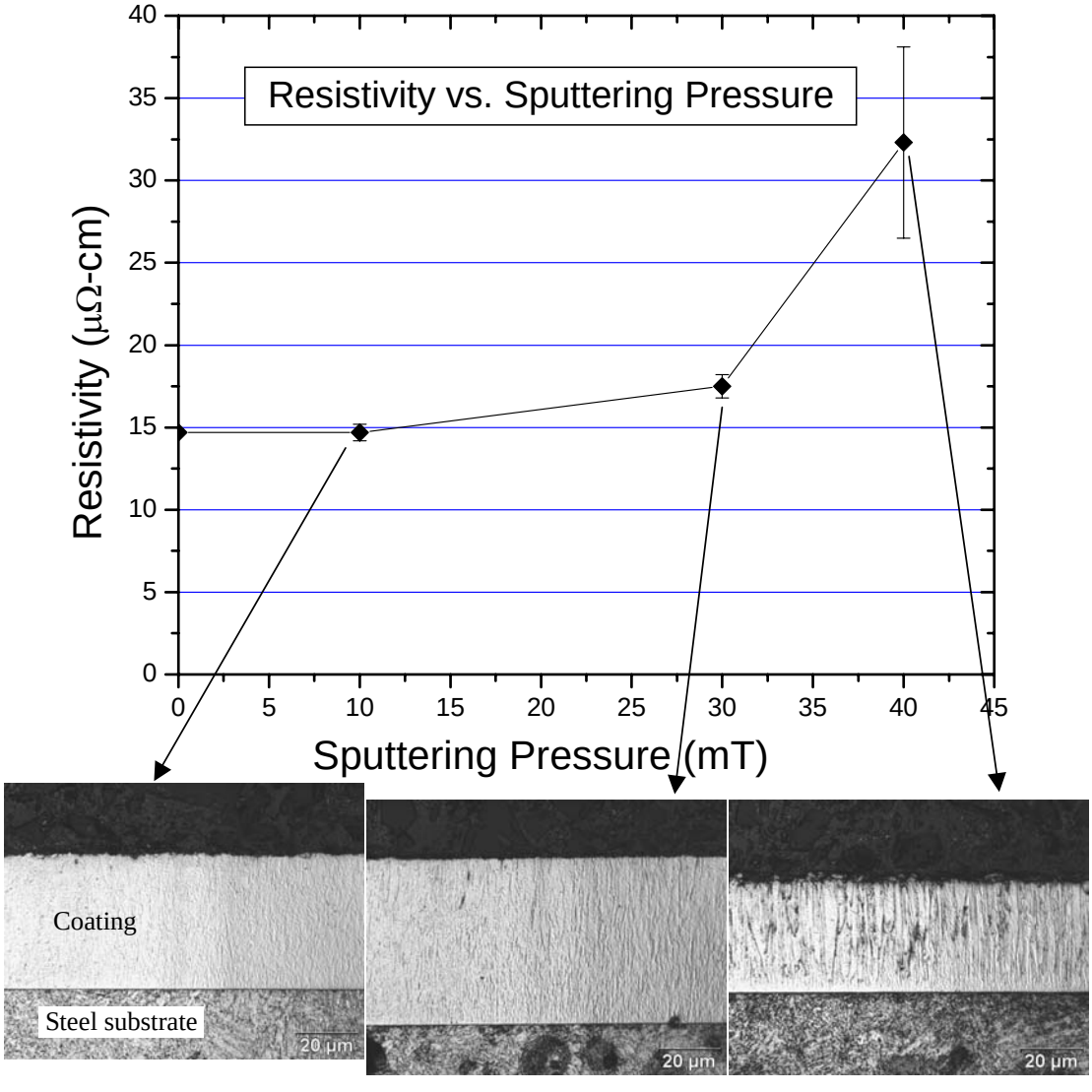

Figure 11. Chart of the resitivity vs. sputtering pressure along with etched metallographic cross sections taken for the niobium

samples sputtered at different pressures. The changes in resistivity correlate well with observed changes in coating porosity.

IV2. The relationship between contamination level and resistivity of coatings for niobium coatings

Two specimens (Nb-A1 and Nb-A2) were deposited to test the correlation of resistivity and coating impurity levels. As stated in the procedure, impurity level was regulated using a controlled leak and an Inficon residual gas analyzer. The results of the scans are given below. Overall, the resistivity scans indicate a fairly uniform value across the samples. There is a much more visible correlation between resistivity and background gas pressure than there is for the case of sputtering pressure. As expected, there is an increase in resistivity of the coatings as background gas pressure is increased. For a residual impurity level of 5% process gas, there is greater than a factor of two increase in resistivity. For 10% process gas impurity levels, there is approximately a factor of six increase. This indicates that the eddy current decay method of resistivity measurement is extremely sensitive to coating contamination levels.

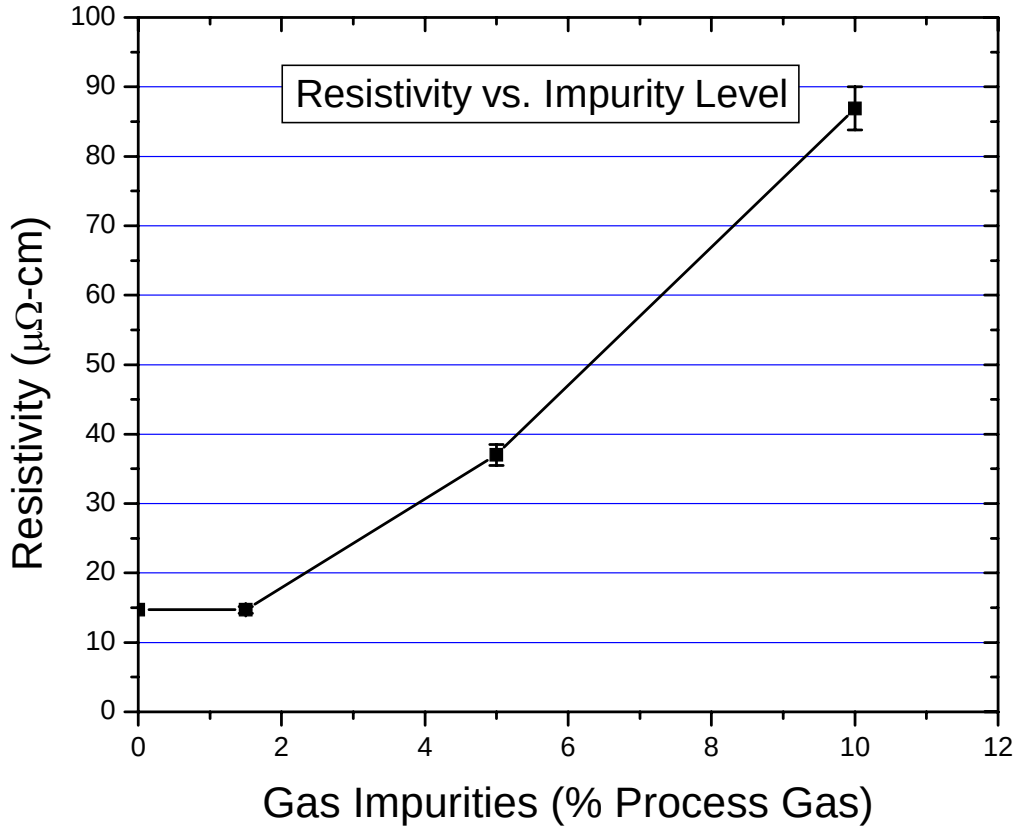

Figure 12. Chart of resistivity vs. impurity level for niobium samples deposited at varying background gas impurity levels.

To ensure that the change in resistivity is in fact due to changes in impurity content and is not strongly effected by changes in porosity, topographic images were taken are shown in Figure 13. As indicated in Figure 13, the coating is a near fully dense structure similar to that of the other specimens sputtered at 10 mT. This indicates that the resistivity changes are indeed due solely to the change in impurity contents and not changes in density.

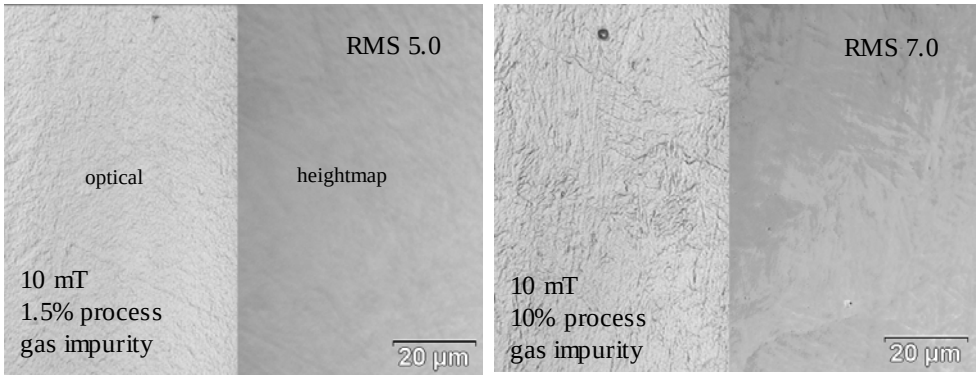

Figure 13 Composite optical and topographic heightmap images as measured by laser scanning confocal microscopy. The sputtering pressure, surface finish, and impurity level are given for each image. With very little change in surface finish.

IV3. The relationship between tantalum coating phase and resistivitiy

Two specimens (Ta-1 and Ta-2) were deposited to test the correlation of resistivity and beta-Ta concentrations in magnetron sputtered tantalum.

The resistivity scan indicates that the resistivity measurement is very sensitive to beta-Ta concentration. This is to be expected considering there is an order of magnitude difference in resistivity of alpha-Ta and beta-Ta. To correlate the approximate beta-Ta fraction to the resistivity measurements, metallographic cross-sections were taken and analyzed (shown in Figure 14). The darker phase in the image in Figure 14 corresponds to the softer alpha-Ta while the lighter phase corresponds to beta-Ta. The approximate beta-Ta fractions are extrapolated from the cross-sections by an image analysis system and cross-referenced to their positions on the resistivity scans. The results are given in the chart below. Overall, the resistivity of the sample sputtered at 30 mT was slightly higher than that sputtered at 10 mT for a given beta-Ta fraction. This is similar to the results achieved with the niobium samples and is likely due to slight changes in coating density.

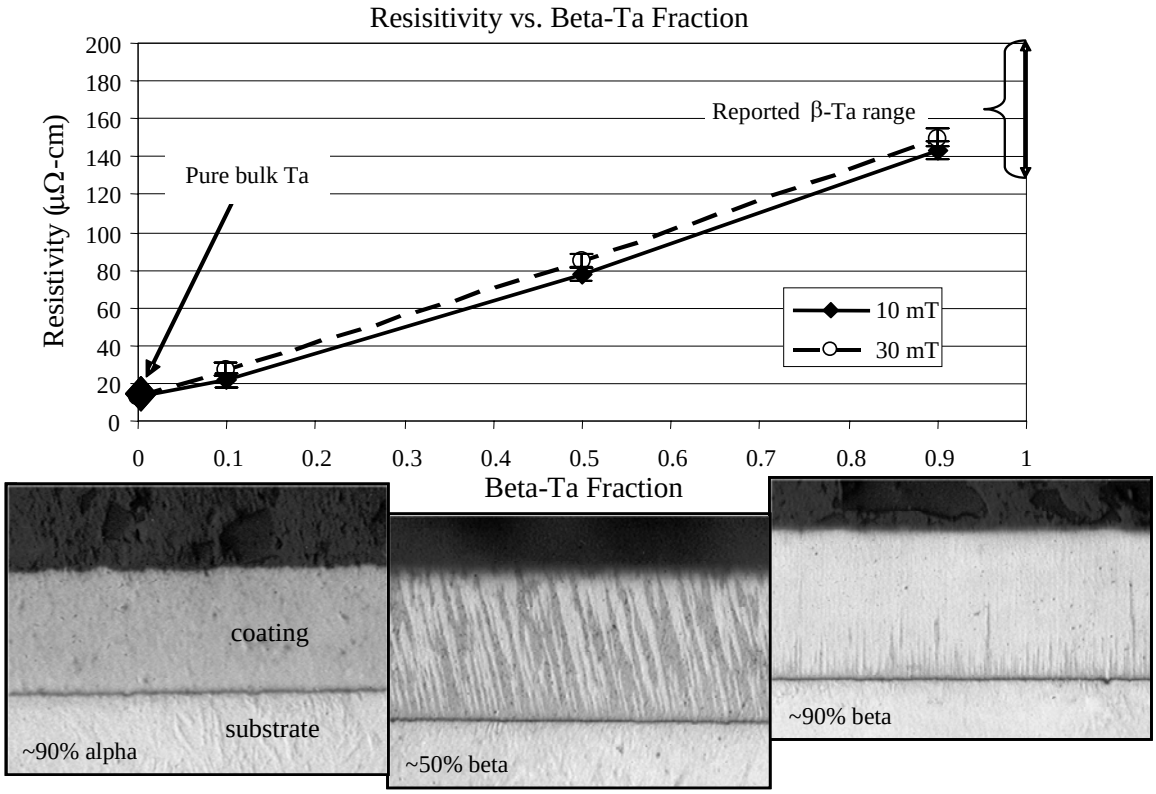

Figure 14 Chart of resistivity vs. beta-Ta fraction for tantalum samples along with representative cross-sections of the coatings taken at areas of varying beta-Ta concentration. The lighter phase denotes alpha-Ta and the darker phase, beta-Ta. Resistivity varies linearly with beta-Ta concentration.

IV4. The relationship between cracking, porosity, and resistivity of thick electroplated chromium coatings

Four specimens of electroplated chromium were completed to determine the correlation between micro-crack density and resistivity. Overall the changes in resistivity were subtle. This is similar to the changes in resistivity observed with changes in coating density, which is not surprising since the phenomenon for resistivity change is nearly identical. That is, the changes in resistivity are essentially due to changes in effective porosity of the coating.

Figure 15 illustrates the overall relationship between micro-crack density as measured by percentage cross-sectional area and resistivity. In addition, micrographs are given of several chromium coatings of varying thickness and micro-crack density.

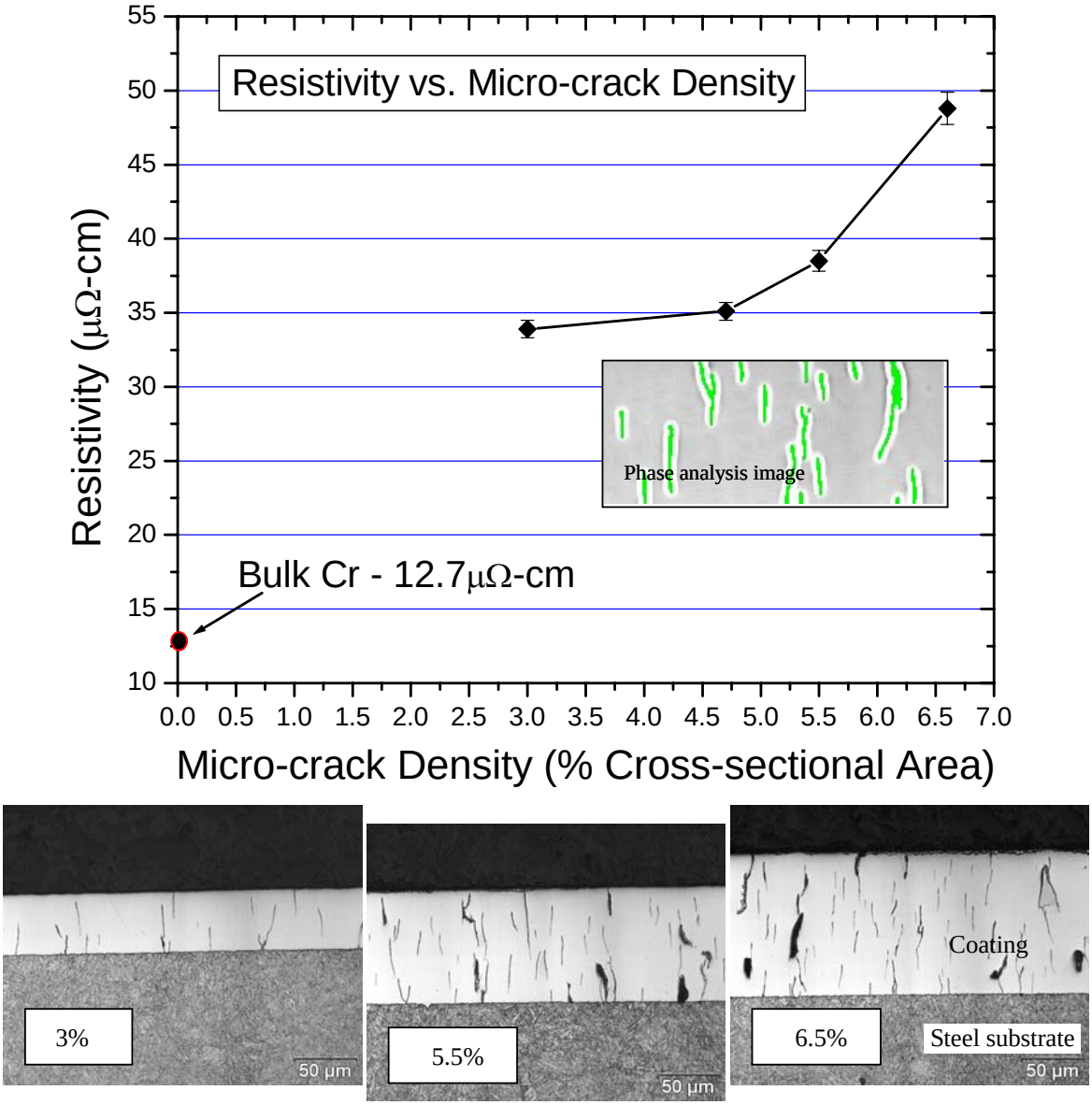

Figure 15 Chart of resistivity vs. micro-crack density for chromium samples along with representative cross-sections of each coating. With increasing coating thickness, the micro-crack density increases along with the resistivity. Resistivity measurements corrected for thickness.

The importance of this relationship can be directly related to the progression of damage in electroplated chromium gun tubes. Figure 16 illustrates the crack widening effect that occurs upon repeated thermal cycles as experienced in gun tubes. This crack widening results in more rapid erosion of the steel interface due to increased vulnerability to the hot propellant gases. This effect should also be accompanied by a change in resistivity that can be measured via eddy current. In this mode, the eddy current method may be utilized to monitor coating degradation levels in the field to determine subsequent wear and erosion life.

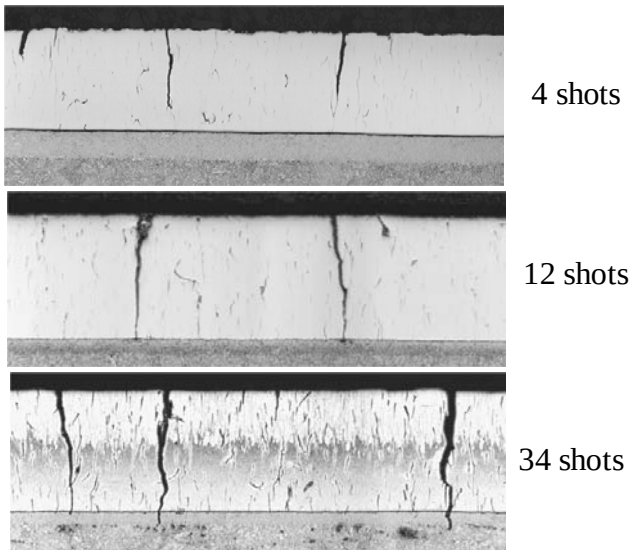

Figure 16. Electroplated HC-Cr Damage Progression in a gun tube erosion simulator. Cross-sectional images taken at 4 shots, 12 shots and 34 shots respectively. The number of large cracks accompanied by subsequent widening will result in changes in resistivity.

IV5. Summary of resistivity measurement results

Table II gives a summary of resistivity measurements acquired all the niobium, tantalum and chromium samples. The measurements are obtained from our 2D scanner and reported here are the average and standard deviations of each sample.

Table II – Average thickness and resistivity, the errors represent the standard deviations

Material	Sample	Average Thickness (μm)		Average Resistivity (μΩ-cm)	
Nb	Nb-A1	40.8 ± 0.7		86.9 ± 3.1	
Nb	Nb-A2	15.9 ± 0.5		37.0 ± 1.5	
Nb	Nb-1	47 ± 1.5		14.7 ± 0.5	
Nb	Nb-2	58 ± 4		17.5 ± 0.7	
Nb	Nb-3	35 ± 4		32.3 ± 5.8	
HC-Cr	Cr-1	44 ± 1		33.9 ± 0.6	
HC-Cr	Cr-2	72 ± 2		35.1 ± 0.6	
HC-Cr	Cr-3	89 ± 3		38.5 ± 0.7	
HC-Cr	Cr-4	137 ± 7		48.8 ± 1.1	
		Alpha phase	Beta phase	Alpha phase	Beta phase
Ta	Ta-1	14 ± 2	29 ± 5	22.7 ± 1.1	149 ± 12
Ta	Ta-2	14 ± 2	30 ± 3	22.2 ± 1.1	143 ± 11

V. Summary And Conclusion

A dual-probe resistivity scanner based on eddy currents was designed and constructed. It was used to determine the resistivity of niobium, tantalum and chromium coatings. The results obtained are in good agreement with other published measurements with other approaches. The pulsed eddy current method was used to develop a technique that allows very fast scan rates with up to 10^5 samples per second. Such scanning capability makes this method useful for coating diagnostics during the manufacturing process and in the field.

In support of the robust and reliable method developed, the following correlations were made: The relationship of impurity level to resistivity is quite dramatic and is easily differentiated utilizing eddy current. The resistivity of niobium coatings vs. sputtering pressure does not follow a linear path. However, based on LSCM results, the resistivity maps of niobium coatings correlate well with density. Excellent correlation was made on resistivity data taken from samples of varying beta-Ta concentration. Resistivity values of tantalum coatings are in good agreement with literature [7][10]. Strong correlation between HC-Cr crack density and resistivity was found. This is useful for both QC testing and measuring coating degradation levels in the field.

References

[1] John C. Moulder, Erol Uzal and James H. Rose, Thickness And Conductivity Of Metallic Layers From Eddy Current Measurements, *Rev. Sci. Instrum.* 63(6), June 1992.

[2] Cheng-Chi Tai, James H. Rose, and John C. Moulder, Thickness And Conductivity Of Metallic Layers From Pulsed Eddy Current Measurements, *Rev. Sci. Instrum.* 67(11), June 1996.

[3] B. Lebrun, Y. Jayet, J. Baboux, Pulsed Eddy Current Signal Analysis: Application To The Experimental Detection And Characterization Of Deep Flaws In Highly Conductive Materials, *NDT & E International* 30(3), pp. 163-170, 1997.

[4] T. Clauzon, F. Thollon and A. Nicolas. Flaws Characterization With Pulsed Eddy Currents N.D.T., *IEEE transactions on Magnetics*, 35(3), May 1999.

[5] S. Giguere, B. Lepine, J. M. S. Dubbis, Pulsed Eddy Current Technology: Characterizing Materials Loss With Gap And Liftoff Variations, *Res Nondestr*, 13, pp. 119-129, 2001.

[6] Y. Danon and C. Lee, Characterization of Ta Thin Coating Using Eddy Current Method, *ASNT spring conference*, pp. 40-41, March, 2003.

[7] Yaron Danon, Changqing Lee, Chris Mulligan and Greg Vigilante, Characterization of Tantalum Sputtered Coatings on Steel Using Eddy Currents, *IEEE transaction on Magnetics, Accepted.*

[8] Jack Blitz, *Electrical And Magnetic Methods Of Non-Destructive Testing*, Chapman & Hall, Second edition, 1997.

[9] J.A. Thornton, The Microstructure of Sputter Deposited Coatings, *Journal of Vacuum Science and Technology A* 4(6), pp. 3059-3065, 1986.

[10] L.A.Clevenger, A.Mutscheller, J.M.E.Harper, C.Cabral, Jr., and K.Barmak, The Relationship Between Deposition Conditions, The Beta To Alpha Phase Transformation, And Stress Relaxation In Tantalum Thin Films, *Journal of Applied. Physics.* 72(10), pp. 4918-4924, 1992.

[11] S.L Lee, D. Windover, M Audino, D.W. Matson, E.D. McClanahan, High-Rate Sputter Deposited Tantalum Coating On Steel For Wear And Erosion Mitigation, *Surface And Coating Technology*, 149, pp. 62-69, 2002.

[12] Philippe Catania, Ronnen A, Roy and Jerome J. Cuomo, Phase Formation And Microstructure Changes In Tantalum Thin Films Induced By Bias Sputtering, *J. Appl. Phys.* 74(2), pp. 1008-1014, 1993.

[13] C. C. Cheng, C. V. Dodd and W.E. Deeds, General Analysis of Probe Coils Near Stratified Conductors, *International journal of nondestructive testing*, 3, pp. 109-130, 1971.

[14] J.A. Thornton, High Rate Thick Film Growth, *Annual Review in Material Science*, 7, pp. 239-260, 1977.

[15] K.H. Muller, Stress and Microstructure of Sputter-deposited Thin Films, *Journal of Applied Physics*, 62, pp. 1796-1799, 1987.